

Precision measurement of cosmic magnification from 21 cm emitting galaxies

Pengjie Zhang¹*, Ue-Li Pen²†

¹*NASA/Fermilab Astrophysics Group, Fermi National Accelerator Laboratory, Box 500, Batavia, IL 60510-050*

²*Canadian Institute for Theoretical Astrophysics, University of Toronto, Toronto, Canada, M5S 3H8*

12 November 2018

ABSTRACT

We show how precision lensing measurements can be obtained through the lensing magnification effect in high redshift 21cm emission from galaxies. Normally, cosmic magnification measurements have been seriously complicated by galaxy clustering. With precise redshifts obtained from 21cm emission line wavelength, one can correlate galaxies at different source planes, or exclude close pairs to eliminate such contaminations.

We provide forecasts for future surveys, specifically the SKA and CLAR. SKA can achieve percent precision on the dark matter power spectrum and the galaxy dark matter cross correlation power spectrum, while CLAR can measure an accurate cross correlation power spectrum. The neutral hydrogen fraction was most likely significantly higher at high redshifts, which improves the number of observed galaxies significantly, such that also CLAR can measure the dark matter lensing power spectrum. SKA can also allow precise measurement of lensing bispectrum.

Key words: Cosmology: large-scale structure of Universe—radio lines: galaxies—galaxies: abundance

1 INTRODUCTION

Gravitational lensing measures the distortion of light by gravity originating from inhomogeneous distribution of matter. The physics of weak gravitational lensing is clean, perhaps comparable to the primary CMB. To the first order approximation, it involves only general relativity and collision-less dark matter dynamics. Gas physics only enters at small scales (Zhan & Knox 2004; White 2004) and can be nulled by throwing away small scale lensing information (Huterer & White 2005). Though the prediction of weak lensing statistics is complicated by nonlinear evolution of matter density fluctuation, high resolution, large box size N-body simulations are able to measure these statistics to high accuracy (e.g. Vale & White (2003); Merz et al. (2005)). Thus, weak gravitational lensing is one of the most powerful and robust tools to constrain cosmology and study the large scale structure of the universe.

Weak gravitational lensing has been detected through cosmic shear (see Refregier (2003) for a recent review). Ongoing and upcoming large scale galaxy surveys such as

CFHTLS¹, DES², LSST³, Pan-STARRS⁴ and SNAP⁵ will reduce the statistical errors of the cosmic shear measurement to $\lesssim 1\%$ level. At that stage, systematic errors such as point spread function, galaxy intrinsic alignment, seeing and extinction (Hoekstra 2004; Jarvis et al. 2004; Vale et al. 2004; van Waerbeke et al. 2004) and errors in galaxy redshift measurement will be ultimate limiting factors. Given these possible systematics, it is worthwhile to search for independent method to measure the gravitational lensing, for consistency check and, for likely better statistical and systematic errors. In this paper, we will show that the cosmic magnification of 21cm emitting galaxies is a competitive candidate.

Cosmic magnification is the lensing induced changes in galaxy number density. It introduces extra correlations in galaxy clustering (Kaiser 1992; Villumsen 1996; Moessner et al. 1998; Jain et al. 2003) and correlates galaxies (quasars) at widely separate redshifts (Moessner & Jain 1998). Cosmic magnification contains as much information of cosmology and matter clustering as cosmic shear.

¹ <http://www.cfht.hawaii.edu/Science/CFHLS/>

² <http://www.darkenergysurvey.org/>

³ <http://www.lsst.org/>

⁴ <http://pan-starrs.ifa.hawaii.edu/public/science/>

⁵ <http://snap.lbl.gov/>

* E-mail:zhangpj@fnal.gov

† E-mail:pen@cita.utoronto.ca

It has been robustly detected in quasar-galaxy lensing (Scranton et al. (2005) and references therein).

The measurement of cosmic magnification does not require the accurate determination of galaxy shapes and is thus free of many systematics, such as point spread function and galaxy intrinsic alignment, entangled in the cosmic shear measurement. But it suffers from several obstacles. (1) It suffers stronger shot noise than cosmic shear measurement. For cosmic shear, shot noise comes from the intrinsic ellipticity of galaxies, which has dispersion $\langle \epsilon^2 \rangle^{1/2} \simeq 0.3$. The shot noise power spectrum is proportional to $\langle \epsilon^2 \rangle / N_g \sim 0.1 / N_g$, where N_g is the total number of galaxies. For cosmic magnification, shot noise comes from the Poisson fluctuation of galaxy counts and the shot noise power spectrum scales as $1/N_g$ and is thus an order of magnitude larger than that in cosmic shear. (2) The signal of cosmic magnification is generally much smaller than intrinsic clustering of galaxies. Without precise redshift measurement of galaxies or quasars, the only method to remove intrinsic clustering of galaxies is to measure the cross correlation of foreground galaxies and background galaxies (or quasars). But its detection is severely limited by the number of high redshift galaxies, which are difficult to detect in optical band, and quasars, which are rare, comparing to galaxy abundance. Early measurements of cosmic magnification were often controversial. Even with relatively large sample of quasars and foreground galaxies from 2dF and SDSS, the measurement of cosmic magnification is still at its infancy and is only confirmed to $\leq 8\sigma$ confidence level.

Besides the observational difficulties, the theoretical prediction of cross correlation strength is complicated by foreground galaxy bias, which is hard to predict from first principles. Without precise understanding of the galaxy bias, the power of cosmic magnification to constrain cosmology and matter distribution is severely limited, compared to cosmic shear.

Cosmic magnification measured from 21cm emitting galaxies is free of many obstacles entangled in the cosmic shear measurement and quasar-galaxy cosmic magnification measurement. As we will show in §2, upcoming radio surveys such as Square Kilometer Array (SKA)⁶ can find $\sim 10^8$ - 10^9 HI-rich galaxies in total and $\sim 10^7$ galaxies at $z > 2$ through the neutral hydrogen 21cm hyperfine transition line. With this large sample of galaxies, the measurement of cosmic magnification will enter the precision era, due to following reasons. (1) Radio observations are free of extinction. Since dust is associated with galaxies, extinction is correlated with foreground galaxies and thus is likely able to produce a false quasar-galaxy or galaxy-galaxy cross correlation signal. (2) Contrary to optical surveys, redshifts of these galaxies can be precisely determined by the redshifted wavelength of the 21cm hyperfine transition line, with no added observational cost. Precision measurement of galaxy redshift is required for the precision prediction of lensing statistics. It also allows the luxury of removing close galaxy pairs, which is crucial to measure cosmic magnification in the presence of the strong auto correlation of galaxies. (3) At high redshift the magnification effect is enhanced, since galaxies at higher redshifts are more strongly lensed and have a steeper flux distribu-

tion. Combined with the large sample of galaxies, shot noise can be overcome. (4) The auto correlation function of cosmic magnification can be measured to high accuracy. The prediction of the cosmic magnification auto correlation is free of galaxy bias prior and as robust as the prediction of cosmic shear power spectrum.

The goal of this paper is modest, which is to demonstrate the feasibility to do precision lensing measurement using 21cm emitting galaxies. Methods discussed in this paper are by no mean optimal and results presented are conservative. Efforts toward optimizing lensing measurement is presented in the companion paper(Zhang & Pen 2005), where we show that cosmic magnification of 21cm emitting galaxies can not only do better than of cosmic magnification optical galaxies, but also can likely do better than cosmic shear of optical galaxies.

Throughout this paper, we adopt a flat Λ CDM universe with $\Omega_m = 0.3$, $\Omega_\Lambda = 1 - \Omega_m$, $\sigma_8 = 0.9$, $h = 0.7$ and initial power index $n = 1$, as is consistent with WMAP result (Spergel et al. 2003). We take Canadian Large Adaptive Reflector (CLAR)⁷ and SKA as our targets to forecast the ability of future radio 21cm surveys to measure cosmic magnification. The instrumental parameters and survey patterns of these two surveys have not been completely fixed yet. For CLAR, we adopt a system temperature $T_{\text{sys}} = 30$ K, effective collecting area $A_{\text{eff}} = 5 \times 10^4 \text{ m}^2$ and field of view 1 deg^2 . For SKA, we adopt the same value of T_{sys} and field of view and adopt $A_{\text{eff}} = 6 \times 10^5 \text{ m}^2$.

2 DETECTING GALAXIES IN RADIO SURVEYS

Though the universe is highly ionized, there are still large amounts of neutral gas present in galaxies. The typical HI mass is around $\sim 10^9 M_\odot$ (Zwaan et al. 1997). HI rich galaxies appear in the radio band by emitting the 21 cm hyperfine line resulting from the transition of atomic hydrogens from spin 1 ground state to spin zero ground state. The spontaneous transition rate is $A_{21} = 2.85 \times 10^{-15} \text{ s}^{-1}$.

Each emission line has negligible width. But since neutral gas has rotational and thermal motions, the integrated intrinsic line width is not negligible. It turns out that the line width of 21 cm emission is mainly determined by the rotation of HI gas, which has a typical velocity $\sim 100 \text{ km/s}$. The Doppler effect by thermal motions cause a velocity width $w \sim c\sqrt{k_B T/m_H} \lesssim 10\sqrt{T/10^4 \text{ K}} \text{ km/s}$. The actual emission line width is determined by many parameters, such as the total mass of galaxies, redshift and inclination angle of the HI disk. For simplicity, we assume that the combined intrinsic line width is $w = 100 \text{ km/s}$. The choice of w affects the prediction of detection efficiency of HI emitting galaxies. But the results shown in this paper should not be changed significantly by more realistic choice of w .

Since the velocity (frequency) resolution of radio surveys can be much higher than the intrinsic line width, the observed flux could have a nontrivial dependence on the bandwidth, whose modeling requires detailed description of HI distribution in galaxies. To avoid this complexity, we adopt

⁶ <http://www.skatelescope.org/>

⁷ <http://www.clar.ca/>

bandwidth to be larger or equal to redshifted 21cm line width, which changes from w at z to $w/(1+z)$ at $z=0$, or in frequency space, to $\Delta\nu = w\nu_{21}/c(1+z)$, where $\nu_{21} = 1.4$ Ghz is the 21cm frequency. The total 21 cm flux of HI rich galaxies is

$$\begin{aligned} S_{21} &= \frac{g_2 A_{21}}{g_1 + g_2} \frac{N_{\text{HI}} E_{21}}{4\pi D_L^2(z)} \left(\frac{w}{c} \frac{\nu_{21}}{1+z} \right)^{-1} \\ &= 0.023 \text{mJy} \frac{M_{\text{HI}}}{10^{10} M_{\odot}} \left(\frac{c/H_0}{\chi(z)} \right)^2 \frac{100 \text{km/s}}{w(1+z)}. \end{aligned} \quad (1)$$

Here, $g_1 = 1$ and $g_2 = 3$ are the degeneracies of atomic hydrogen spin 0 and 1 ground state. $E_{21} = h\nu_{21}$ is the energy of each 21cm photon. $N_{\text{HI}} = M_{\text{HI}}/m_{\text{HI}}$ is the total number of neutral hydrogen of a galaxy with total hydrogen mass M_{HI} . $D_L(z) = \chi(z)(1+z)$ is the luminosity distance and χ is the comoving angular distance. $H_0 = 100h \text{ km/s/Mpc}$ is the Hubble constant at present time.

Instrumental noise scales as $\Delta\nu^{-1/2}$, where $\Delta\nu$ is the bandwidth. So a larger bandwidth helps to beat down instrumental noise. But if the bandwidth is larger than the 21 cm line width, the signal is diluted and scales as $1/\Delta\nu$. Thus, the highest signal to noise ratio is gained when the bandwidth $\Delta\nu$ is equal to the redshifted bandwidth of integrated 21cm emission line, $w\nu_{21}/c(1+z)$. The system noise per beam is

$$\begin{aligned} S_{\text{sys}} &= \frac{\sqrt{2} T_{\text{sys}}}{\eta_c A_{\text{eff}}} \frac{k_B}{\sqrt{\Delta\nu t}} \\ &\simeq 0.032 \text{mJy} \frac{T_{\text{sys}}}{30 \text{K}} \frac{5 \times 10^4 \text{m}^2}{A_{\text{eff}}} \left(\frac{100 \text{km/s}}{w/(1+z)} \frac{\text{hour}}{t} \right)^{1/2}. \end{aligned} \quad (2)$$

Here, η_c is the correlator efficiency, which is adopted as $\eta_c = 0.9$. The instrumental beam area is $A_b \sim \lambda^2/A_{\text{eff}}$. For CLAR, $A_b \simeq 10'^2 (\nu_{21}/\nu)^2$. For SKA, $A_b \simeq 1'^2 (\nu_{21}/\nu)^2$. 21cm emitting regions have typical size $\sim 30 \text{kpc/h}$ or $\sim 1''$ at $z \sim 1$. Thus, the size of 21cm emitting regions is much smaller than the beam size. The observed flux is thus the total flux of each galaxies. In this case, the calculation of the detection threshold is straightforward.

If we choose those peaks with flux above nS_{sys} (n - σ selection threshold), the minimum HI mass selected is

$$\begin{aligned} M_{\text{HI},\text{min}} &= n \times 1.39 \times 10^{10} M_{\odot} \left(\frac{\chi(z)}{c/H_0} \right)^2 (1+z)^{3/2} \\ &\times \sqrt{\frac{w}{100 \text{km/s}}} \frac{\text{hour}}{t} \frac{T_{\text{sys}}}{30 \text{K}} \frac{5 \times 10^4 \text{m}^2}{A_{\text{eff}}}. \end{aligned} \quad (3)$$

We assume that the HI mass function follows the Schechter function found at $z=0$ (Zwaan et al. 1997)

$$n(M, z) dM = n_0(z) \left(\frac{M}{M_*(z)} \right)^{-\gamma} \exp \left(-\frac{M}{M_*(z)} \right) dM. \quad (4)$$

We fix $\gamma = 1.2$. Zwaan et al. (1997) found that $M_*(z=0) = 10^{9.55} h^{-2} M_{\odot}$ and $n_0(z=0) = 0.014 h^3 \text{Mpc}^{-3}$. There is little solid measurement of $n_0(z)$ and $M_*(z)$ other than at local universe. But for this form of the mass function, there exists a tight relation between Ω_{HI} , the cosmological neutral hydrogen density with respect to the present day critical density, and $n_0 M_*$:

$$\Omega_{\text{HI}} h = 2.1 \times 10^{-4} \frac{n_0(z)}{n_0(z=0)} \frac{M_*(z)}{M_*(z=0)}. \quad (5)$$

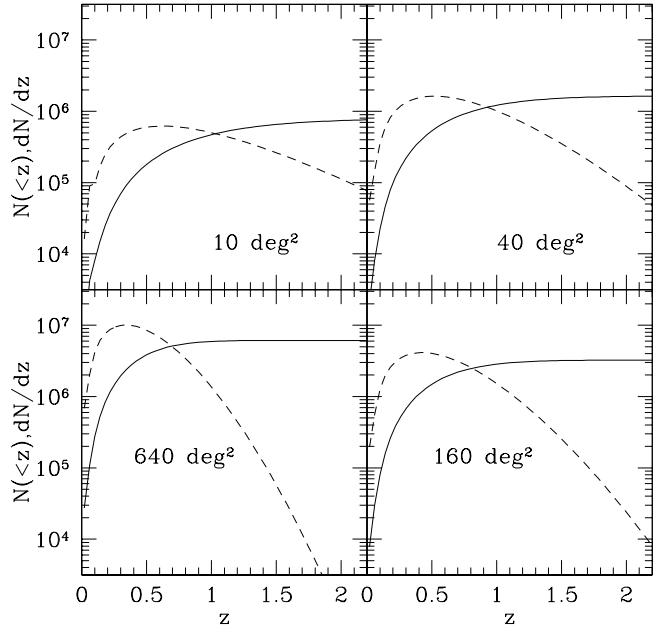


Figure 1. The predicted abundance of 21cm emitting galaxies above 4σ detection threshold of CLAR 5 year survey. The solid lines are the cumulative number distribution $N(< z)$ and the dashed lines are the differential distribution dN/dz . The total number of observed galaxies is of the order 10^6 and the number of galaxies at $z > 1$ is of the order 10^5 . We assume no evolution in the mass function. If realistic evolution model is considered, the total number of galaxies at $z > 1$ can increase by a factor of 5 or more.

Observations of damped Lyman- α systems and Lyman- α limit systems measure Ω_{HI} from $z=0$ to $z \sim 4$. Combining Eq. 5 and these observations, one can put constraints on n_0 and M_* . These observations found that Ω_{HI} increases by a factor of 5 toward $z \sim 3$ and then decreases toward higher redshift (Zwaan et al. (1997); Rao & Turnshek (2000); Storrie-Lombardi & Wolfe (2000); Péroux et al. (2003) and data compilation in Péroux et al. (2003); Nagamine et al. (2004)). Either the increase of n_0 or M_* increases the detectability of 21cm emitting galaxies. Thus, estimations based on the assumption of no evolution should be regarded as conservative results. We will show that even in this conservative case, future radio surveys such as CLAR and SKA still allow precise measurement of galaxy-galaxy lensing (§3) and in the case of SKA, the precise measurement of lensing power spectrum (§3 & 4) and lensing bispectrum (§5). If we adopt evolution models implied by and consistent with observations, even CLAR is able to measure the lensing power spectrum (§6).

The number of galaxies detected depends on the selection threshold n . If we choose 4σ detection threshold ($n=4$), CLAR could detect $\sim 10^6$ - 10^7 galaxies in a 5-year survey. A deeper survey (smaller sky coverage) detects a larger fraction of high redshift galaxies. But since the survey volume is smaller, the total number of high redshift galaxies is not necessarily higher. A survey area around 100 deg^2 is optimal to detect high z galaxies. For a 160 deg^2 survey area, $\sim 10^6$ galaxies at $z > 1$ can be detected. SKA is about 10

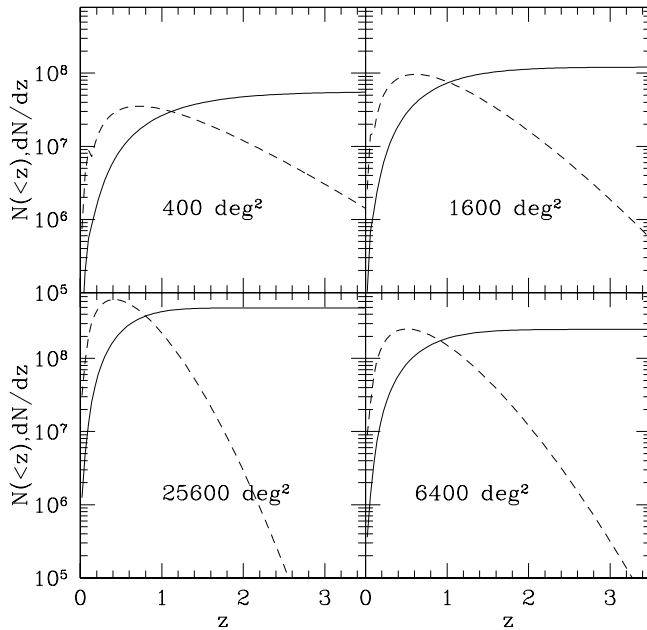


Figure 2. Similar as Fig. 1, but for SKA 5 year survey. The total number of observed galaxies is of the order 10^8 and the number of galaxies at $z > 1$ is of the order 10^7 . We assume no evolution in the mass function. If a realistic evolution model is considered, the total number of galaxies at $z > 1$ can increase by a factor of 5 or more.

times more sensitive than CLAR and can detect two orders of magnitude more galaxies. For a 1600 deg^2 survey area, $\sim 10^8$ galaxies at $z > 1$ and $\sim 10^7$ galaxies at $z > 2$ can be detected. As a reminder, these estimations are extremely conservative. The number of galaxies detected at $z > 1$ can be enhanced by a factor of 5 or more if the evolution effect is considered.

Some peaks above the selection threshold are caused by noise. N_{noise} , the number of false peaks, has strong dependence on the detection threshold. If we choose $n = 1$ (1σ detection), the number of false peaks of noise is

$$N_{\text{noise}} \sim \frac{4\pi f_{\text{sky}}}{A_{\text{pixel}}} \frac{\nu}{\Delta v} \frac{\text{Erfc}(1.0/\sqrt{2})}{2} \lesssim 10^{10} f_{\text{sky}} \frac{1}{A_b} . \quad (6)$$

For CLAR deep surveys which cover $f_{\text{sky}} \sim 1\%$ of the sky, $N_{\text{noise}} \lesssim 10^7$, which is still less the number of detected galaxies above 1σ threshold. For SKA with several thousand square degree sky coverage, N_{noise} above 1σ is $\sim 10^8$, which is slightly less than the total number of galaxies above 1σ threshold. In CMB measurements, signal-to-noise per pixel is often chosen to be 1, which maximizes return on the power spectrum measurement. This would correspond to a detection threshold for which the false-positive rate is 50%. In this sense, we can choose $n = 1$ as our selection threshold. The selection threshold problem can be dealt with in a more sophisticated way. The survey measures a three-dimensional map of the sky. Each pixel in that map will have some significance of detection. Clearly the large number of low significance pixels do collectively contain information, if they can be averaged in a meaningful way. Zhang & Pen (2005) de-

scribe one such algorithm to extract the luminosity function deep into the noise.

With these large samples of galaxies, the galaxy clustering can be precisely measured. This allows constraining cosmology through the baryon oscillation (Abdalla & Rawlings 2005). The redshift distortion of galaxies allows the measurement of galaxy velocity power spectrum to high accuracy⁸. In this paper we do not attempt to utilize all information of these galaxies. Our primary goal is to demonstrate the feasibility of using future 21cm radio survey to do precision lensing measurement. We notice that the properties of lensing magnification depends strongly on the mass threshold or equivalently n . We will explore different $n \geq 1$ to find suitable choice for different quantities. For $n \gtrsim 3$, since the number of false peaks is much smaller than the number of detected galaxies, one can safely neglect all errors caused by false detections. But for $n \lesssim 3$, one has to take them into account.

3 CROSS CORRELATIONS OF DIFFERENT REDSHIFT BINS

3.1 Cosmic magnification preliminary

Cosmic magnification changes the galaxy number over-density δ_g to⁹

$$\delta_g^L = \delta_g + 2(\alpha - 1)\kappa + O(\kappa^2) . \quad (7)$$

Here, $\alpha \equiv -f'(> F_c)F_c/f(F_c)$, $f(> F)$ is the number of galaxies brighter than F , F_c is the flux limit adopted and κ is the lensing convergence. Since $\langle \kappa \rangle = 0$, to the accuracy of $\langle \kappa^2 \rangle \sim 10^{-4}$, lensing does not change the averaged $f(> F)$. Thus α is effectively an observable.

The usual method to eliminate the intrinsic correlation of close galaxy pairs is to cross correlate galaxies in two separate redshift bins. Galaxy peculiar velocity shifts the position of galaxies in the redshift space by $c\Delta z \lesssim 10^3 \text{ km/s}$. Galaxy correlation becomes negligible at scales $r \gtrsim 100h^{-1} \text{ Mpc}$, which corresponds to $\Delta z \sim 0.03[H(z)/H_0][r/100h^{-1} \text{ Mpc}]$. Choosing $\Delta z \gtrsim 0.05$, residual correlations caused by intrinsic galaxy correlation can be safely neglected. With accurate measurement of 21cm emitting galaxy redshift, this can be done straightforwardly.

The distribution of foreground galaxies traces lenses of background galaxies which cause the magnification effect. Thus there exists a correlation between the background magnification and foreground galaxies. This galaxy-galaxy correlation is the correlation generally considered in the literature. There exists another correlation. Both foreground galaxies and background galaxies are lensed by intervening matter. Thus there exists the background magnification-foreground magnification correlation. The combined correlation is

$$\begin{aligned} \langle \delta_g^L(\theta_f, z_f) \delta_g^L(\theta_b, z_b) \rangle &= 2(\alpha_b - 1)\langle \kappa_b \delta(\theta_f, z_f) \rangle \\ &+ 4(\alpha_f - 1)(\alpha_b - 1)\langle \kappa_f \kappa_b \rangle . \end{aligned} \quad (8)$$

⁸ Zhang & Pen, 2005, in preparation

⁹ In this expression, we neglect all high order terms throughout this paper. These terms increase the lensing signal (Ménard et al. 2003a) and thus improve the correlation measurement.

Here the subscript f and b denote foreground and background respectively. The first term in the right side of the equation is the magnification-galaxy correlation and the second term is the magnification-magnification correlation.

The observed galaxy surface density is

$$\Sigma_g = \int_{z_{\min}}^{z_{\max}} n_g(z)(1 + \delta^L)dz. \quad (9)$$

Its correlation function is Eq. 8 weighted by the differential galaxy number distribution n_g and clustering signal. By Limber's approximation, the corresponding 2D angular power spectrum of the magnification-galaxy cross correlation is given by

$$\frac{l^2 C_l^{\mu g}}{2\pi} = \frac{3\Omega_m H_0^2}{2c^2} N_f^{-1} \frac{\pi}{l} \times \int_{z_{f,\min}}^{z_{f,\max}} \Delta_{gm}^2 \left(\frac{l}{\chi_f}, z_f \right) G_b(z_f) n_g(z_f) \chi_f dz_f. \quad (10)$$

Here, Ω_m is the present day matter density with respect to the cosmological critical density. $N_f = \int n_g(z_f) dz_f$ is the total number of foreground galaxies. $\Delta_{gm}^2 = b_g r_g \Delta_m^2$ is the galaxy-matter cross correlation power spectrum. We assume $b_g r_g = 1$ (b_g is the galaxy bias and r_g is the cross correlation coefficient between galaxies and dark matter). The matter power spectrum Δ_m^2 is calculated using the BBKS transfer function (Bardeen et al. 1986) and its non-linear evolution is calculated by Peacock-Dodds fitting formula (Peacock & Dodds 1996). G_b , the kernel of the background magnification effect, is given by

$$G_b(z) = \frac{1+z}{N_b} \int_{z_{b,\min}}^{z_{b,\max}} w(\chi, \chi_b) n_g(z_b) 2(\alpha(z_b) - 1) dz_b. \quad (11)$$

Here, $w(\chi, \chi_b)$ is the lensing geometry function. For the flat universe we adopt, the geometry function is simplified to $w(\chi, \chi_b) = \chi(1 - \chi/\chi_b)$. The strength of the magnification effect relies on both the strength of lensing, which prefers background galaxies with higher z , and $\alpha - 1$, which prefers deeper slope of the mass function at the mass threshold.

The power spectrum of the corresponding magnification-magnification cross correlation is:

$$\frac{l^2 C_l^{\mu\mu}}{2\pi} = \left(\frac{3\Omega_m H_0^2}{2c^2} \right)^2 \frac{\pi}{l} \times \int_0^{z_{f,\max}} \Delta_m^2 \left(\frac{l}{\chi}, z \right) G_f(z) G_f(z) \chi d\chi. \quad (12)$$

Here, G_f , the kernel of foreground magnification effect, is given by

$$G_f(z) = \frac{1+z}{N_f} \int_{z_{f,\min}}^{z_{f,\max}} w(\chi, \chi_f) n_g(z_f) 2(\alpha(z_f) - 1) dz_f \quad (13)$$

where N_f is the total number of foreground galaxies. The amplitude of $C_l^{\mu\mu}$ relies on both the lensing signal of foreground and background galaxies. The higher the z_f and z_b , the stronger the correlation signal. It also depends strongly on $\alpha_f - 1$ and $\alpha_b - 1$. If the mass threshold is larger, $\alpha - 1$ is generally larger.

Depending on the choice of foreground bins and foreground galaxy selection criteria (which determines α and thus the strength of magnification effect), either $C_l^{\mu g}$ or $C_l^{\mu\mu}$ can dominate. In §3.2, we discuss cases where $C_l^{\mu g}$ dominates and in §3.3, we discuss cases where $C_l^{\mu\mu}$ dominates.

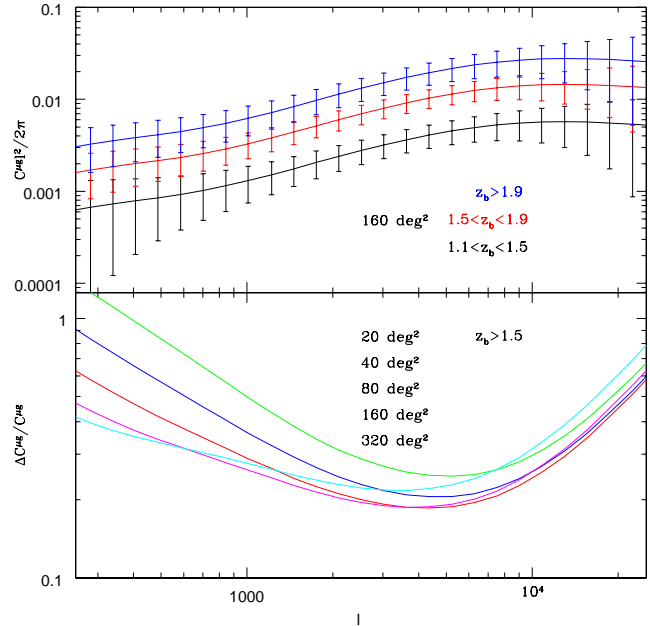


Figure 3. The predicted accuracy of cosmic magnification-galaxy cross correlation power spectrum $C^{\mu g}$ measured by CLAR 5 year survey. Foreground galaxies ($0.5 < z_f < 1.0$) are selected with a 2σ selection threshold. The optimal survey coverage is around several hundred square degrees. For such configuration, $C^{\mu g}$ can be measured to $\sim 20\%$ accuracy at l around several thousand (lower panel, bin size $\Delta l = 0.2l$). $C^{\mu\mu}$ is several percent of $C^{\mu g}$ and does not show up in the plot. In top panel, we further split background galaxies into several redshift bins. This lensing tomography allows the measure of the evolution of matter distribution. It also allows the measure of relative change of the comoving distance as a function of z to better than 10% in three redshift bins at $z_b > 1$.

3.2 Magnification-galaxy power spectrum

For a sufficiently wide foreground galaxy redshift distribution with low median redshift, the lensing effect and the magnification ($\alpha - 1$) effect are both small. Generally, in this case, $C_l^{\mu\mu}$ is much smaller than $C_l^{\mu g}$. In this section, we fix the foreground galaxy distribution ($0 < z_f < 1.0$) and vary the background galaxy redshift distribution. For this choice of foreground galaxy distribution, $C^{\mu\mu}$ is $\sim 1\%$ of $C^{\mu g}$ (Fig. 4). The correlation signal peaks at $l \simeq 10^4$, where the fluctuation is $\sim 10\%$.

$C_l^{\mu g}$ is the projection of Δ_{gm}^2 along the line of sight (Eq. 10). Given a cosmology, $\Delta_{gm}^2(k, z)$ can be extracted using the inversion methods applied to galaxy surveys and lensing surveys (e.g. Dodelson et al. (2002); Pen et al. (2003b)). $\Delta_{gm}^2(k, z)$ contains valuable information of galaxy clustering and can put strong constraint on halo occupation distribution.

Cosmological information is also carried in the geometry term of lensing, in our case, χ in $C^{\mu g}$ and $C^{\mu\mu}$. By fixing the foreground galaxy distribution and varying the background galaxy distribution, one can isolate χ_b from Δ_{gm}^2 and measure the dependence of χ_b on z_b . This method allows an independent and robust constraint on cosmology (Jain et al. 2003; Zhang et al. 2003).

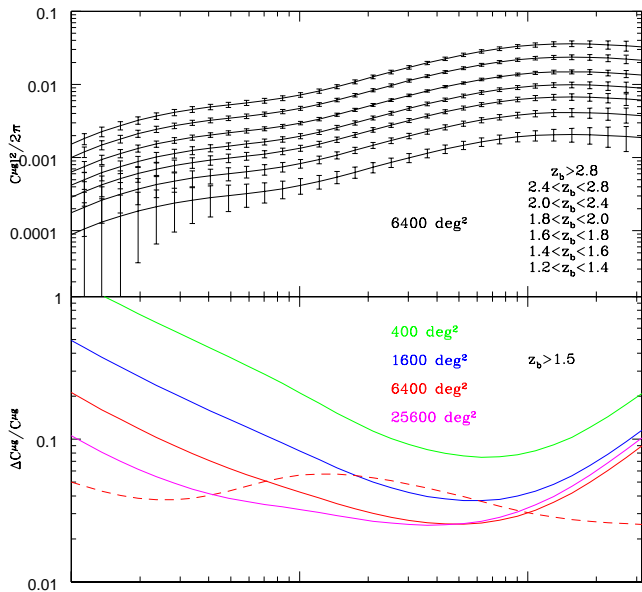


Figure 4. Similar as Fig. 3, but for SKA 5 year survey. Foreground galaxies are chosen to be at $0.7 < z_f < 1.0$. To measure $C^{\mu g}$, optimal sky coverage should be around ten thousand degrees. Under such configuration, $C^{\mu g}$ can be measured to several percent accuracy at $1000 \lesssim l \lesssim 10^4$. The dashed line in the lower panel is $C^{\mu \mu} / C^{\mu g}$ for 6400 deg^2 sky coverage. The dependence of comoving distance $\chi(z)$ on redshift can be measured to be better than 1% in 7 redshift bins at $z > 1$.

The statistical error in the $C^{\mu g}$ measurement¹⁰ is

$$\Delta C_l^{\mu g} = \sqrt{\frac{C_{\mu g}^2 + (C_g^b + C_{\text{shot}}^b)(C_g^f + C_{\text{shot}}^f)}{(2l + 1)\Delta l f_{\text{sky}}}}. \quad (14)$$

Here, C_g^b is the auto correlation power spectrum of the background galaxies, which includes contributions from $\langle \delta_g^b \delta_g^b \rangle$, $\langle \kappa_b \kappa_b \rangle$ and $\langle \delta_g^b \kappa_b \rangle$. For high redshift background galaxies, $\langle \kappa_b \kappa_b \rangle$ is not negligible comparing to the intrinsic galaxy correlation $\langle \delta_g^b \delta_g^b \rangle$ and thus has to be taken into account. $C_{\text{shot}}^b = 4\pi f_{\text{sky}}[1 + N_{\text{noise}}^b / N_b]/N_b$ is the background shot noise power spectrum. The extra factor $1 + N_{\text{noise}}^b / N_b$ accounts for the contaminations of false peaks in the selected background sample. These false peaks does not correlate with each other, so their only effect is to increase the shot noise. For selection thresholds above $2-\sigma$, false positive rate is small and this extra factor can be neglected. C_g^f is the auto correlation power spectrum of the foreground galaxies.

Statistical errors strongly depend on f_{sky} (when fixing total observation time). This dependence is complicated. (1) f_{sky} affects $\alpha(z_f)$. Shorter integration time per unit area is required in order to survey for a larger sky area. This in-

¹⁰ At frequencies below 1.4 Ghz, radio sources have smooth continuum spectra, so they can be subtracted away in the frequency space (Wang et al. 2005). Their only effect is to contribute to T_{sys} and cause a fluctuation in T_{sys} across the sky. This can introduce a false correlation, but it is routine in observation to eliminate this effect and thus we do not consider it in this paper.

creases system noise per beam and thus increases the selection mass threshold of high z galaxies. Since the mass function is steeper at higher mass, $\alpha(z_f)$ increases and $C^{\mu g}$ increases. (2) f_{sky} affects the relative distribution of galaxies. Larger f_{sky} survey detects relatively more low z galaxies. Since $C_l^{\mu g}$ is proportional to Δ_{gm}^2 weighted by the distribution of foreground galaxies and matter clustering is stronger at lower z , larger sky coverage tends to increase $C^{\mu g}$. But on the other hand, the lensing effect is smaller for lower z galaxies. This has the effect to decrease $w(\chi, \chi_b)$ and thus decrease $C^{\mu g}$. Furthermore, the noise terms C_g^b and C_g^f increase. (3) f_{sky} affects the cosmic variance. (4) f_{sky} affects the total number of foreground and background galaxies and thus changes the shot noise. The lower panels of fig. 3 & 4 show the dependence of $\Delta C_l^{\mu g} / C_l^{\mu g}$ on sky coverage. If the sky coverage is too small, the cosmic variance is large. If the sky coverage is too large, too few background galaxies can be detected. Shot noise begins to dominate at relatively large scales. The choice of selection threshold n ($n-\sigma$) also affects the statistical errors. Larger n increases α and thus increases $C^{\mu g}$. But it also decreases the number of detected galaxies and thus increases shot noise.

Both CLAR and SKA can measure $C^{\mu g}$ precisely (fig. 3 & 4). For CLAR, the optimal sky coverage is around several hundred square degree. $C^{\mu g}$ can be measured to $\sim 20\%$ accuracy for bin size $\Delta l = 0.2l$. It can also measure $C^{\mu g}$ at several redshift bins and allows isolating geometry. For SKA, the optimal sky coverage is around ten thousand square degree. $C^{\mu g}$ can be measured to $\sim \%$ accuracy. The size of background redshift bins can be as narrow as $\Delta z \lesssim 0.1$. The change of $\chi_b(z)$ can be precisely measured at $z \gtrsim 1$.

The best result from optical galaxy surveys by far is an 8σ detection by SDSS, using an optimal quasar weighting function (Scranton et al. 2005). CLAR will detect much less galaxies and cover much smaller sky area, but even CLAR can reach $\sim 5-\sigma$ at more than 10 independent bins of width $\Delta l = 0.2l$. If adopted similar background galaxy weighting function, the result can be further improved. So CLAR and SKA can do much better than optical galaxy surveys. This is well explained by Eq. 14. (1) The number of $z > 1$ CLAR galaxies is of the order 10^6 and is much higher than the number of SDSS quasars ($\sim 2 \times 10^4$). This significantly reduces the shot noise term C_{shot}^b in Eq. 14. (2) CLAR foreground galaxies have broad redshift distribution, which roughly matches the lensing kernel of background galaxies and thus amplifies the cross correlation signal. For SDSS, quasars lie at $z \gtrsim 1$ while most galaxies locate at $z \ll 0.5$. Since these quasars are mainly lensed by matter at $z \gtrsim 0.5$, the cross correlation signal is weak and $C^{\mu g} \ll \sqrt{C_g^b C_g^f}$. This is likely the dominant reason why the measured cross correlations by 2dF and SDSS (Myers et al. 2003; Scranton et al. 2005) do not have as good S/N as one would naively expect from their large galaxy and quasar samples.

It is difficult for optical surveys to detect large number of high z galaxies. But 21cm radio surveys can. This is an inherent advantage of 21cm radio surveys to measure cosmic magnification. Furthermore, since 21cm galaxies have precise redshift measurement, one can weight foreground galaxies deliberatively to optimize the cross correlation mea-

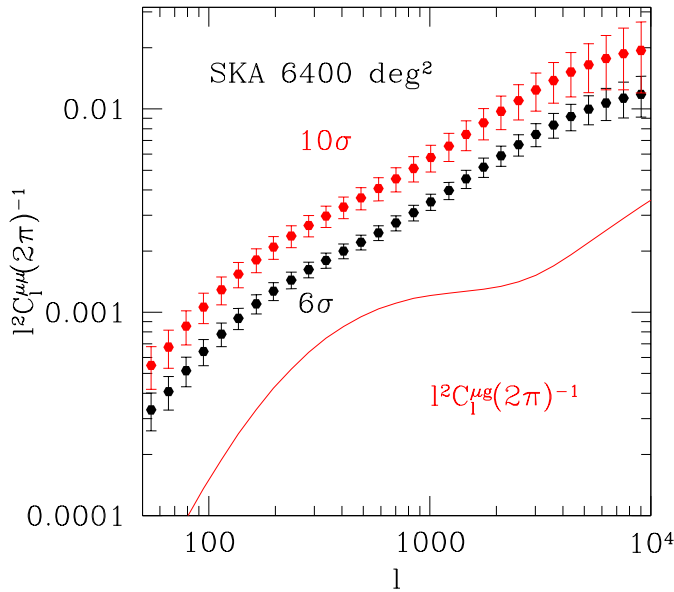


Figure 5. The predicted accuracy of $C_l^{\mu\mu}$, magnification-Magnification cross correlation power spectrum in two redshift bins, by SKA 5 year surveys. The measurement of $C_l^{\mu\mu}$ allows constraining cosmology and studying matter clustering without the complexity of galaxy bias. We choose foreground galaxies at $1.6 \leq z_f \leq 2.0$ and background galaxies at $2.0 \leq z_b \leq 4.0$. We treat $C_l^{\mu g}$ as contaminations. Since $C_l^{\mu\mu}$ depends on $\alpha - 1$ of foreground galaxies while $C_l^{\mu g}$ does not, we vary the selection threshold of foreground galaxies to change $C_l^{\mu\mu}/C_l^{\mu g}$. We fix the selection threshold of background galaxies as 4σ . For 6σ and 10σ selection threshold of foreground, galaxies, systematic errors ($C_l^{\mu g}$) is comparable to statistical errors (error-bars of data points).

surement. This is another inherent advantage of 21cm radio surveys.

3.3 Magnification-Magnification power spectrum

The main strength of the cosmic shear power spectrum and bispectrum to constrain cosmology lies in the fact that the prediction of these quantities only relies on the matter clustering whose theoretical understanding is robust. The prediction of $C_l^{\mu\mu}$ is as straightforward as the prediction of the cosmic shear power spectrum, which does not require the knowledge of complicated galaxy bias, as $C_l^{\mu g}$ does. So, the measurement of $C_l^{\mu\mu}$ would allow robust constraints on cosmological parameters and dark matter clustering, as cosmic shear power spectrum does. In this section, we will show that SKA is straightforward to measure the magnification (foreground)-magnification (background) cross correlation power spectrum $C_l^{\mu\mu}$.

For the purpose of constraining cosmology using $C_l^{\mu\mu}$, $C_l^{\mu g}$ should be treated as contamination and marginalized over. $C_l^{\mu\mu}$ depends on the magnification strength of foreground galaxies, while $C_l^{\mu g}$ does not. By increasing the redshifts of foreground galaxies, the lensing signal increases and $\alpha - 1$ also increases, due to higher mass selection threshold

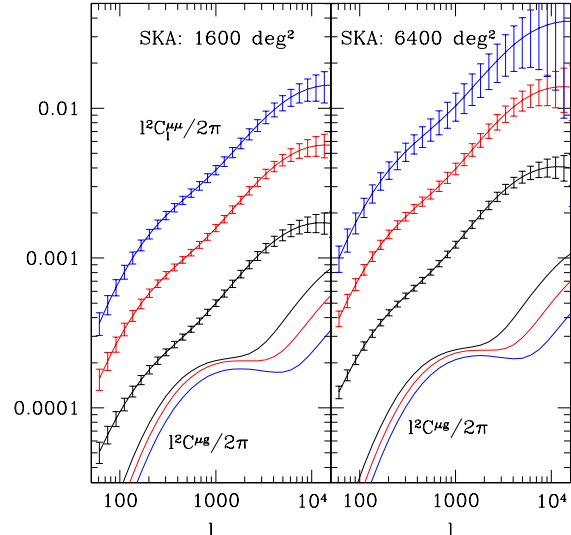


Figure 6. Auto correlation angular power spectrum of galaxies. We disregard close pairs within redshift separation $\Delta z < 0.1$ and thus eliminate intrinsic galaxy clustering. We try different galaxy distribution. Lines with error bars, from bottom to top, correspond to $z > 1.5$, $z > 2.0$, and $z > 2.5$, respectively. For our choice of 4σ selection threshold and $z > 1.5$, $C_l^{\mu\mu}$ dominates over $C_l^{\mu g}$. For higher redshift, the luminosity function is steeper at the limiting flux. Larger $\alpha - 1$ then increases $C_l^{\mu\mu}$ with respect to $C_l^{\mu g}$. On the other hand, high redshift galaxies are mainly lensed by low z matter distribution. The higher the redshift, the less likely that galaxies can be lensed by matter distribution in the same redshift bins. This also increase $C_l^{\mu\mu}$ with respect to $C_l^{\mu g}$. We assume no evolution in the HI mass function. Realistic evolution scenarios would result in more galaxies and thus allow better measurement.

at higher redshift, thus $C_l^{\mu\mu}$ increases with respect to $C_l^{\mu g}$. Since $C_l^{\mu g}$ is proportional to the strength of matter clustering, it decreases when increasing redshifts of foreground galaxies. But these requirements to increase $C_l^{\mu\mu}$ with respect to $C_l^{\mu g}$ can be at odds with the requirement to reduce statistical errors. For example, increasing the mass selection threshold or redshifts of foreground galaxies reduces N_f and thus increases shot noise.

We try different foreground redshift bins, selection threshold and sky coverage to optimize the measurement of $C_l^{\mu\mu}$ such that $C_l^{\mu g}/C_l^{\mu\mu}$ is smaller or comparable to the statistical error. For SKA, it is indeed possible to measure $C_l^{\mu\mu}$ and control both systematic errors ($C_l^{\mu g}$) and statistical errors to 10% level (Fig. 5). Since such measurement requires large number of high z galaxies, it is extremely difficult for optical surveys to realize it.

4 AUTO CORRELATION

With the precision measurement of galaxy redshift and large amount of high z galaxies, one can extract the cosmic magnification from the galaxy auto correlation measurement. In the correlation estimator, we throw away pairs with redshift separation $|z_1 - z_2| \leq \Delta z_c$. We choose $\Delta z_c = 0.1$, which corresponds to comoving separation $r_c \simeq 180h^{-1}\text{Mpc}$ at $z = 1$

and $r_c \simeq 100h^{-1}\text{Mpc}$ at $z = 2$. In Fourier space, this corresponds to cut off the power at $k_c \lesssim 1/r_c \lesssim 0.01h/\text{Mpc}$. Applying the Limber's equation in Fourier space, the angular fluctuation at multipole l is contributed by the spacial fluctuation at $k = l/\chi$. Then an effective cut off k_c in Fourier space corresponds to an effective cutoff at $l_c = k_c\chi \lesssim 20$. So, under the Limber's approximation, one can neglect the residual intrinsic correlation of galaxies at $l \gtrsim 20$.

One can further quantify the residual intrinsic clustering. The angular correlation it produces is

$$w_{\text{IC}}^c(\theta) = 2 \int_{z_{\text{min}}}^{z_{\text{max}}} n_g^2(z) \frac{dz}{d\chi/dz} \times \int_{r_c}^{\infty} \xi_g(\sqrt{\chi^2\theta^2 + (\Delta\chi)^2}, z) d\Delta\chi. \quad (15)$$

Here, ξ_g is the galaxy correlation function. Numerical calculation shows that $|w_{\text{IC}}^c(\theta)|$ is smaller than 10^{-5} at all scales. For example, $|w_{\text{IC}}^c(\sim 1')|$ is less than $\sim 10^{-5}$ and $|w_{\text{IC}}^c(\sim 1^\circ)|$ is less than several $\times 10^{-7}$. One can further convert $w_{\text{IC}}^c(\theta)$ to the corresponding C_l . We find that $|l^2 C_l/(2\pi)| \lesssim 10^{-5}$ at all scales. Specifically, at $l \sim 100$, $|l^2 C_l/(2\pi)| \lesssim \text{several} \times 10^{-6}$ and at $l \sim 1000$, $|l^2 C_l/(2\pi)| \lesssim \text{several} \times 10^{-6}$. The angular fluctuation caused by residual galaxy intrinsic clustering is roughly 1% of $C^{\mu\mu}$ at $l \sim 100$ and much less than 1% at smaller scales. So, the close pair removal procedure effectively eliminates all intrinsic galaxy clustering.

The auto correlation function is composed of two parts, the one arising from the auto correlation of cosmic magnification and the one from the cross correlation between cosmic magnification and δ_g . The magnification auto correlation power spectrum is

$$\frac{l^2 C_l^{\mu\mu}}{2\pi} = \left(\frac{3\Omega_m H_0^2}{2c^2} \right)^2 \frac{\pi}{l} \int_0^{z_{\text{max}}} \Delta_m^2 \left(\frac{l}{\chi}, z \right) G(z)^2 f_2^2(z) \chi d\chi \quad (16)$$

where N is the total number of galaxies in the corresponding redshift bin. This expression differs from Eq. 12 only by a factor $f_2^2(z)$, which arises from the close pair removal. $f_2(z)$ is given by

$$f_2^2(z) = \left[\frac{(1+z)}{NG(z)} \right]^2 \int 4w(\chi, \chi_1)(\alpha_1 - 1)w(\chi, \chi_2)(\alpha_2 - 1) \times n_g(z_1)n_g(z_2)\Theta(|z_1 - z_2| - \Delta z_c) dz_1 dz_2. \quad (17)$$

The function $\Theta(x) = 0$ if $x < 0$ and $\Theta(x) = 1$ if $x > 0$. $G(z)$ is defined analogous to G_b and G_f .

The power spectrum of the magnification-galaxy cross correlation function is

$$\frac{l^2 C_l^{\mu g}}{2\pi} = \frac{3\Omega_m H_0^2}{2c^2} N^{-1} \frac{\pi}{l} \int_{z_{\text{min}}}^{z_{\text{max}}} \times \Delta_{gm}^2 \left(\frac{l}{\chi(z)}, z \right) G(z) f_1(z) n_g(z) \chi(z) dz. \quad (18)$$

The effect of close pair removal is carried by $f_1(z)$

$$f_1(z) = \frac{1+z}{NG(z)} \int_{z_{\text{min}}}^{z_{\text{max}}} w(\chi, \chi_b) \times n_g(z_b)(\alpha(z_b) - 1)\Theta(|z_b - z| - \Delta z_c) dz_b. \quad (19)$$

Again, as explained in 3.3, for the purpose of constraining cosmology, we treat $C^{\mu g}$ as contaminations of $C^{\mu\mu}$. For the SKA, both the statistical errors of $C^{\mu\mu}$ and systematics errors ($C^{\mu g}$) can be controlled to better than 10% level, if we

only use $z \gtrsim 1.0$ galaxies (Fig. 6). For CLAR, the detectability of $C^{\mu\mu}$ is sensitive to the evolution of HI mass function. Assuming the conservative no evolution model, $C^{\mu\mu}$ can be detected at the several σ level (fig. 8). Though this close pair removal method is successful for 21cm emitting galaxies, it is essentially infeasible for optical galaxies because of (1) insufficient number of high z optical galaxies and (2) inaccurate photo-z redshifts and too expensive spectroscopic redshifts.

5 COSMIC MAGNIFICATION BISPECTRUM

Lensing bispectrum contains valuable and often complimentary information on cosmology and the large scale structure, comparing to the 2-point correlation power spectrum (Bernardeau et al. 1997; Hui 1999; Bernardeau et al. 2002; Ménard et al. 2003b; Pen et al. 2003a; Takada & Jain 2004). But current data only allows low significance detection of the skewness at several angular scales (Bernardeau et al. 2002; Pen et al. 2003a; Jarvis et al. 2004). 21cm radio surveys can do much better. In this section, we will show its feasibility by focusing on the bispectrum of galaxies in the same redshift bins. We throw away close pairs with $|z_i - z_j| < 0.1$ where z_i ($i = 1, 2, 3$) is the redshift of each galaxies.

The bispectrum comes from four parts, $\langle \mu\mu\mu \rangle$, $\langle \mu\mu g \rangle$, $\langle \mu gg \rangle$ and $\langle ggg \rangle$. The $\langle \mu gg \rangle$ and $\langle ggg \rangle$ terms are negligible following similar argument in §4. The $\langle \mu\mu\mu \rangle$ term contributes a bispectrum

$$B_{\mu\mu\mu}(l_1, l_2, l_3) = \left(\frac{3\Omega_m H_0^2}{2c^2} \right)^3 \int_0^{z_{\text{max}}} G^3(z) f_3^3(z) \chi^{-4} \times B_\delta \left(\frac{l_1}{\chi}, \frac{l_2}{\chi}, \frac{l_3}{\chi}; \chi \right) d\chi. \quad (20)$$

Here, $f_3(z)$ takes the effect of close pair removal into account. $B_\delta(k_1, k_2, k_3; \chi)$ is the matter density bispectrum, which is calculated adopting the fitting formula of Scoccimarro & Couchman (2001).

The $\langle \mu\mu g \rangle$ term contributes another bispectrum

$$B_{\mu\mu g}(l_1, l_2, l_3) = 3 \left(\frac{3\Omega_m H_0^2}{2c^2} \right)^2 \int_{z_{\text{min}}}^{z_{\text{max}}} G^2(z) f_4^2(z) \chi^{-4} \times b_g B_\delta \left(\frac{l_1}{\chi}, \frac{l_2}{\chi}, \frac{l_3}{\chi}; \chi \right) \frac{n_g(z)}{N} dz. \quad (21)$$

Here, $f_4(z)$ takes the effect of close pair removal into account. We explicitly show the galaxy bias b_g in the above equation, though we adopt $b_g = 1$ in the estimation. The factor 3 comes from the permutation of $\langle \mu_i \mu_j g_k \rangle$.

The shot noise of the bispectrum is

$$B_{\text{shot}}(l_1, l_2, l_3) = C_N^2 + C_N(C_1 + C_2 + C_3). \quad (22)$$

Here, $C_N = 4\pi f_{\text{sky}}/N$ is the shot noise power spectrum. Full evaluation of the sample variance of bispectrum involves integrating 6-point nonlinear density correlation function. Since we do not have robust theoretical predictions or simulation results of 6-pt nonlinear correlation function, we only consider the Gaussian sample variance. The statistical error of corresponding bispectrum B_{123} is

$$\Delta B_{123} = \sqrt{\frac{2}{N_{123}}} (C_1 C_2 C_3 + B_{\text{shot}}^2). \quad (23)$$

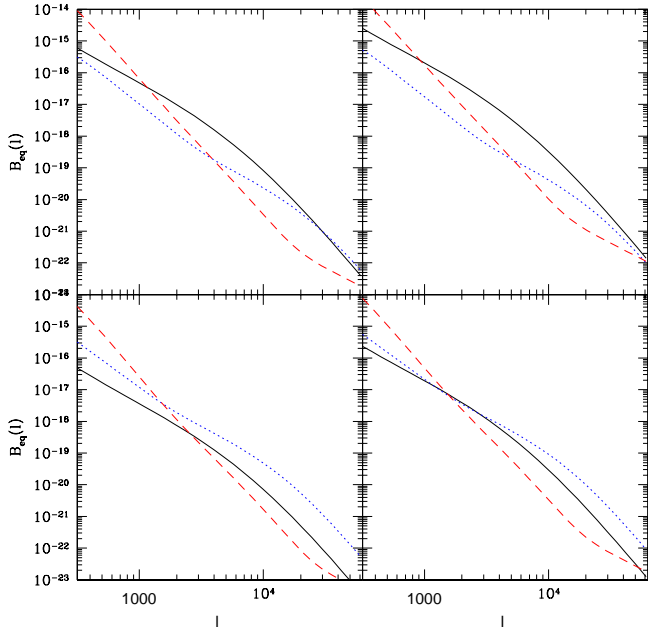


Figure 7. Forecasted measurement of bispectrum by SKA. We assume no evolution in the HI mass function. The solid lines are $B_{\mu\mu\mu}$ of equilateral configuration ($l_1 = l_2 = l_3$), the dot lines are $B_{\mu\mu g}$ and the dash lines are the statistical error. For statistical error, we adopt the l bin size $\Delta l = 0.2l$ and the angular bin size 10° . We try different galaxy redshift ranges and selection thresholds. The top left, top right, bottom left and bottom right panels are the results of $(3\sigma, z > 1.5)$, $(5\sigma, z > 1.5)$, $(3\sigma, z > 1.0)$ and $(5\sigma, z > 1.0)$, respectively.

Here, $C_i = C^{\mu\mu}(l_i) + C^{\mu g}(l_i)$. N_{123} is the number of independent combination of l_1, l_2, l_3 used to obtain the averaged B_{123} . For a rectangle survey area with x axis size θ_x and y axis size θ_y , independent modes are $\mathbf{l} = (2\pi m/\theta_x, 2\pi n/\theta_y)$, where $m, n = 0, \pm 1, \pm 2, \dots$. There is a constraint that $l_3 = -l_1 - l_2$, then the total number of independent combination is

$$\begin{aligned} N_{123} &= dm_1 dn_1 dm_2 dn_2 \\ &= \left(\frac{\theta_x}{2\pi} \frac{\theta_y}{2\pi}\right)^2 l_1 dl_1 l_2 dl_2 2\pi d\theta_{12} \end{aligned} \quad (24)$$

where θ_{12} is the angle between \mathbf{l}_1 and \mathbf{l}_2 . We only show the result of $\mathbf{l}_1 \simeq \mathbf{l}_2 \simeq \mathbf{l}_3$, for which, we choose $\Delta l = 0.2l$ and $\Delta\theta_{12} = \pi/18$ (10°).

At large scales ($l \lesssim 1000$), cosmic variance prohibits the measurement of $B_{\mu\mu\mu}$ and $B_{\mu\mu g}$. But at scales $l \sim 10^4$, either $B_{\mu\mu\mu}$ or $B_{\mu\mu g}$ or both can be measured to be better than 10% accuracy by SKA (Fig. 7). As expected, higher z and/or higher selection threshold result in higher lensing signal and amplify $B_{\mu\mu\mu}$ with respect to $B_{\mu\mu g}$. The computation of three point function may appear computationally challenging, requiring the enumeration of N^3 triangles with $N \sim 10^8$. Recently, linear algorithms have been devised which resolve these problems (Zhang & Pen 2005). Again the requirements of precise redshift measurement and high z galaxies prohibit the measurement of lensing bispectrum through cosmic magnification of optical galaxies.

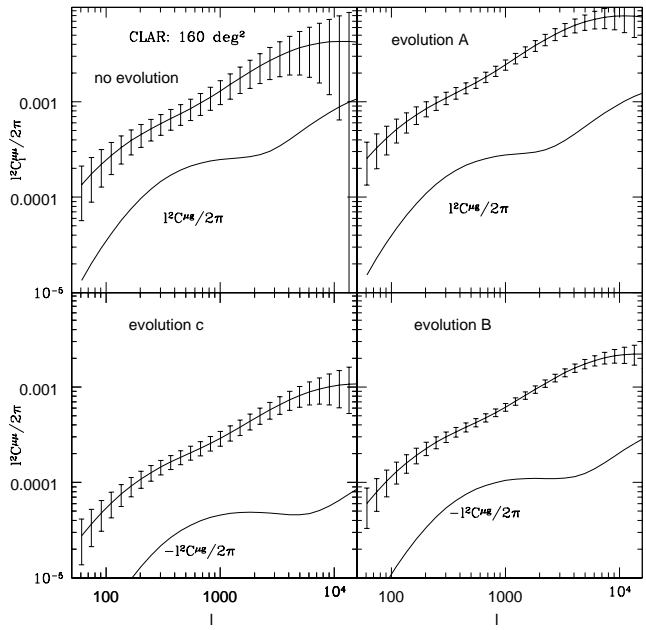


Figure 8. $C^{\mu\mu}$ and $C^{\mu g}$ that would be measured in the same redshift bin by CLAR. We try different evolution models, as explained in §6. Top left panel assumes no evolution and we choose galaxies selected above 2σ at $z > 1.5$. Other panels assume evolution models explained in the text. Top right panel uses galaxies above 3σ at $z > 1.5$. Bottom right panel uses galaxies above 2σ at $z > 2.0$, Bottom left panel uses galaxies above 1σ at $z > 2.5$.

6 EVOLUTION EFFECT

We have demonstrated the feasibility of measuring lensing power spectra and bispectrum in cross correlation of galaxies in two redshift bins and in auto correlation of galaxies in the same redshift bin. We caution on that these results (fig. 1, 2, 3, 4, 5 & 6, 7) should be regarded as conservative estimation of the power of radio surveys to measure cosmic magnification. There are several reasons. One is that in this paper we only use galaxies in certain redshift ranges and above certain selection threshold. Better measurement of $C^{\mu\mu}$ and $C^{\mu g}$ can be obtained by cross correlating galaxies above 1σ detection threshold at all redshifts. To estimate how much can one gain requires the design of careful weighting on different redshifts and luminosity (HI mass). This work is beyond the scope of this paper. Another reason is that we have assumed no evolution in the HI mass function. Evolution effect is very likely to improve the accuracy of lensing measurement by providing many more detected galaxies. We will investigate the evolution effect in this section.

As discussed in §2, the observed $\Omega_{\text{HI}}h$ shows a factor of 5 increase from $z = 0$ to $z \sim 3$. Its evolution can be approximated as $g(z) = (1+z)^{2.9} \exp(-z/1.3)$. Thus we have a constraint of $n_0(z)M_*(z) = n_0(z=0)M_*(z=0)g(z)$. There is little solid constraint on the evolution of n_0 or M_* separately. But the observation of damped Lyman- α systems and Lyman-Limit systems provides some indirect constraints. Damped Lyman- α systems have HI column density $N_{\text{HI}} \geq 2 \times 10^{20} \text{ cm}^{-2}$. If the size of the corresponding HI regions is $\sim 30 \text{ kpc}/h$, then the total HI mass is $\sim 10^{10} M_\odot$.

Thus these damped Lyman- α systems are likely part of corresponding massive HI (proto-)galaxies. On the other hand, Lyman-Limit systems have much smaller HI column density and are likely part of less massive HI galaxies. The ratio of damped Lyman- α systems abundance with respect to Lyman-limit systems decreases after $z = 3$. This implies that there may be fewer massive HI galaxies after $z \sim 3$ and thus an evolution of $M_*(z)$.

Since the constraint to either n_0 or M_* is weak and it is likely that both $n_0(z)$ and $M_*(z)$ evolve, we explore three evolution scenarios. (A) No evolution in $M_*(z)$. $n_0(z) = n_0(z=0)g(z)$. (B) No evolution in $n_0(z)$. $M_*(z) = M_*(z=0)g(z)$. (C). $n_0(z)/n_0(z=0) = M_*(z)/M_*(z=0) = g(z)^{1/2}$.

The number of $z > 1$ galaxies increases by at least a factor of 5 for these evolution scenarios. Taken the evolution effect into account, even CLAR can measure $C^{\mu\mu}$ to $\sim 10\%$ accuracy (systematic and statistical, fig. 8).

7 DISCUSSION

We further address that the results shown in this paper only utilize a small fraction of cosmic magnification information contained in 21cm emitting galaxy distribution. (1) We only tried several bins of galaxy redshift distribution and several galaxy selection threshold to demonstrate that cosmic magnification can be measured to high accuracy. To utilize the full lensing information, one needs to divide galaxies into many redshift bins and selection threshold bins. One then measures (N-point) auto correlation functions of each bins and cross correlation functions between different bins. In principle, one can develop optimal weighting scheme to combine all measurements to get the best measurement of lensing statistics and lensing-galaxy statistics. (2) We did not attempt to separate the cosmic magnification auto correlations and the cosmic magnification-galaxy correlations. These two classes of correlation have different dependence on the selection threshold of galaxies. These dependences are straightforward to predict and can be applied to separate two components. Such component separation improves the robustness of constraining cosmology and large scale structure significantly. The cosmic magnification auto correlations and the geometry of cosmic magnification-galaxy correlations (Jain et al. 2003; Zhang et al. 2003) are ideal to constrain cosmology and matter clustering. The amplitude and angular scale dependence cosmic magnification-galaxy correlations are ideal to constrain halo occupation distribution. Advanced analysis methods are required to address the above two issues and to utilize full information of cosmic magnification information in 21cm emitting galaxy distribution. (3) We note that individual galaxies can be resolved with SKA, this allows the measurement of cosmic shear. It may also allow an independent measure of cosmic magnification. SKA resolution allows the measurement of an inclination angle. If galaxies at high redshift also follow a Tully-Fisher relation, the lensing effect can also be large compared to shot noise and can be extracted. Since we do not know the evolution of the scatter in the Tully-Fisher at high redshift, we do not use this information in this paper. It is likely that real surveys can do significantly better than our estimates.

Utilizing all information of cosmic magnification information in 21cm emitting galaxy distribution, the relative er-

ror of cosmic magnification will be much smaller than what shown in this paper. Upon this precision era, one needs to improve the theoretical prediction to better than 1% accuracy and at the same time, understand possible 1% systematics.

Our prediction of cosmic magnification is simplified in two ways. (1) We only considered the leading order term of cosmic magnification (Eq. 7). Higher order terms are known to be capable of generating 10% effect (e.g. Ménard et al. (2003a)) and have to be included to interpret data at the forecast accuracy. (2) For the lensing convergence, we neglected high order corrections caused by lens-lens coupling and deviation from Born's approximation. These high order corrections are known to have several percent effect (Schneider et al. 1998; Vale & White 2003; Dodelson & Zhang 2005) and should be taken into account.

Source-lens coupling (Bernardeau 1998; Hamana 2001) can have non-negligible effect to cosmic shear. It arises from the fact that measured cosmic shear is always weighted by the number of observed galaxies, which also trace the matter distribution. But this effect does not exist in cosmic magnification where we directly correlate the numbers of observed galaxies at two different redshifts and directions.

Several other approximations in our cosmic magnification measurement only introduce negligible corrections. (1) we have assumed that the luminosity function $f(> F)$ is the same everywhere and thus α is the same everywhere. This picture is over simplified. $f(> F)$ can have environmental dependence. Thus in principle $\langle \alpha\alpha \rangle \neq \langle \alpha \rangle^2$. This affects the prediction of correlations where two or more cosmic magnification terms present (e.g. in $C^{\mu\mu}$, $B_{\mu\mu\mu}$ and $B_{\mu\mu g}$). But this effect is very small, since α only depends on local environment, for two redshift bins with modest separation $\Delta z \gtrsim 0.05$, $\langle \alpha_1\alpha_2 \rangle \simeq \langle \alpha_1 \rangle \langle \alpha_2 \rangle$. The close pair removal procedure further guarantees that even for the same redshift bin, $\langle \alpha_1\alpha_2 \rangle \simeq \langle \alpha_1 \rangle \langle \alpha_2 \rangle$. Thus, one can safely neglect this effect. (2) Residual intrinsic clustering causes $\sim 1\%$ correction at $l \sim 100$ (§4)¹¹. Since cosmic variance at $l \sim 100$ is $\gtrsim 0.01 f_{\text{sky}}^{-1/2}$. One needs to worry about this effect only for full sky surveys. Furthermore, it can be reduced by extrapolating galaxy correlation function ξ_g at smaller scales measured from the same survey to relevant scales ($\gtrsim 100h^{-1}\text{Mpc}$).

8 CONCLUSIONS

We have made simple forecasts for future radio surveys to measure gravitational lensing. We found that radio surveys can be precise sources for lensing measurements, and that lensing magnification is measurable because redshifts are known and many galaxies can be detected. CLAR and SKA are expected to measure the dark matter power spectrum and galaxy-matter cross correlation to high accuracy. The estimates are conservative, since evolution in HI mass function, as suggested by observations, will improve the above results significantly. Also, many effects will increase the sensitivity. Unfortunately, these effects, which include Tully-

¹¹ But it causes $\ll 1\%$ correction at smaller scales.

Fisher relations, are difficult to quantify at high redshifts, for which we neglect in this paper.

More complete statistical information is available at lower signal to noise levels and using non-Gaussian statistics. We have made estimates of the three point statistics, which appear promising, and are expected to improve the information that can be gained by lensing.

Acknowledgments We thank Ron Ekers and Simon Johnston for explanation of radio experiments. We thank Scott Dodelson for helpful discussion. P.J. Zhang was supported by the DOE and the NASA grant NAG 5-10842 at Fermilab.

REFERENCES

Abdalla, F. B., & Rawlings, S. 2005, MNRAS, 360, 27

Bardeen, J. M., Bond, J. R., Kaiser, N., & Szalay, A. S. 1986, ApJ, 304, 15

Bernardeau, F., van Waerbeke, L., & Mellier, Y. 1997, Astron. & Astrophys., 322, 1

Bernardeau, F. 1998, Astron. & Astrophys., 338, 375

Bernardeau, F., Mellier, Y., & van Waerbeke, L. 2002, Astron. & Astrophys., 389, L28

Dodelson, S., et al. 2002, ApJ, 572, 140

Dodelson, S., & Zhang, P. 2005, astro-ph/0501063

Hamana, T. 2001, MNRAS, 326, 326

Hoekstra, H. 2004, MNRAS, 347, 1337

Hui, L. 1999, ApJL, 519, L9

Huterer, D., & White, M. 2005, astro-ph/0501451. submitted to PRD

Jain, B., Scranton, R., & Sheth, R. K. 2003, MNRAS, 345, 62

Jain, B., & Taylor, A. 2003, Physical Review Letters, 91, 141302

Jarvis, M., Bernstein, G., & Jain, B. 2004, MNRAS, 352, 338

Jarvis, M., Jain, B., 2004, astro-ph/0412234

Kaiser, N. 1992, ApJ, 388, 272

Maoli, R., Van Waerbeke, L., Mellier, Y., Schneider, P., Jain, B., Bernardeau, F., Erben, T., & Fort, B. 2001, Astron. & Astrophys., 368, 766

Ménard, B., Hamana, T., Bartelmann, M., & Yoshida, N. 2003, Astron. & Astrophys., 403, 817

Ménard, B., Bartelmann, M., & Mellier, Y. 2003, Astron. & Astrophys., 409, 411

Merz, H., Pen, U., & Trac, H. 2005, New Astronomy. astro-ph/0402443

Moessner, R., Jain, B., & Villumsen, J. V. 1998, MNRAS, 294, 291

Moessner, R., & Jain, B. 1998, MNRAS, 294, L18

Myers, A. D., Outram, P. J., Shanks, T., Boyle, B. J., Croom, S. M., Loaring, N. S., Miller, L., & Smith, R. J. 2003, MNRAS, 342, 467

Nagamine, K., Springel, V., & Hernquist, L. 2004, MNRAS, 348, 421

Peacock, J. A., & Dodds, S. J. 1996, MNRAS, 280, L19

Pen, U., Zhang, T., van Waerbeke, L., Mellier, Y., Zhang, P., & Dubinski, J. 2003a, ApJ, 592, 664

Pen, U., Lu, T., van Waerbeke, L., & Mellier, Y. 2003b, MNRAS, 346, 994

Péroux, C., McMahon, R. G., Storrie-Lombardi, L. J., & Irwin, M. J. 2003, MNRAS, 346, 1103

Rao, S. M., & Turnshek, D. A. 2000, ApJS, 130, 1

Refregier, A. 2003, Annu. Rev. Astron. Astrophys., 41, 645

Schneider, P., van Waerbeke, L., Jain, B., & Kruse, G. 1998, MNRAS, 296, 873

Scoccimarro, R., & Couchman, H. M. P. 2001, MNRAS, 325, 1312

Scranton, R., et al. 2005, astro-ph/0504510, ApJ, accepted

Spergel, D. N., et al. 2003, ApJS, 148, 175

Storrie-Lombardi, L. J., & Wolfe, A. M. 2000, ApJ, 543, 552

Takada, M., & Jain, B. 2004, MNRAS, 348, 897

Vale, C., & White, M. 2003, ApJ, 592, 699

Vale, C., Hoekstra, H., van Waerbeke, L., & White, M. 2004, ApJL, 613, L1

Van Waerbeke, L., et al. 2001, Astron. & Astrophys., 374, 757

Van Waerbeke, L., Mellier, Y., Pelló, R., Pen, U.-L., McCracken, H. J., & Jain, B. 2002, Astron. & Astrophys., 393, 369

van Waerbeke, L., Mellier, Y., & Hoekstra, H. 2004, astro-ph/0406468

Villumsen, J. V. 1996, MNRAS, 281, 369

Wang, X. et al. 2005, astro-ph/0501081

White, M. 2004, Astroparticle Physics, 22, 211

Zhan, H., & Knox, L. 2004, ApJL, 616, L75

Zhang, J., Hui, L., & Stebbins, A. 2003, astro-ph/0312348, submitted to ApJ

Zhang, L. L., & Pen, U.-L. 2005, New Astronomy, 10, 569

Zhang, T. & Pen, U. 2005, astro-ph/0503064

Zhang, P. & Pen, U., 2005, astro-ph/0506740

Zwaan, M. A., Briggs, F. H., Sprayberry, D., & Sorar, E. 1997, ApJ, 490, 173